Available online at www.sciencedirect.com
ScienceDirect
Mechatronics 18 (2008) 282–288
MECHATRONICS

Design and input-shaping control of a novel scanner for high-speed atomic force microscopy

Georg Schitter [a,b,*], Philipp J. Thurner [b], Paul K. Hansma [b]

[a] Delft University of Technology, Delft Center for Systems and Control, Mekelweg 2, 2628 CD, Delft, The Netherlands
[b] University of California Santa Barbara, Physics Department, 6324 Broida Hall, Santa Barbara, CA 93106, USA

Abstract

A novel design of a scanning unit for atomic force microscopy (AFM) is presented that enables scanning speeds three orders of magnitude faster than compared to conventional AFMs. The new scanner is designed for high mechanical resonance frequencies, based on a new scanner design, which is optimized using finite element analysis. For high-speed scanning a new controller, based on input-shaping techniques, has been developed that reduces imaging artifacts due to the scanner's dynamics. The implementation of the new AFM system offers imaging capabilities of several thousand lines per second with a scanning range of 13 μm in both scanning directions, and the freedom to choose the fast scan-axis in any arbitrary direction in the X–Y-plane.

Keywords: AFM; Fast scanning; Nano-positioning; Nanotechnology; Scanning probe; Real-time imaging; Mechanical design

1. Introduction

Nano- and biotechnology are currently very important areas of research. Imaging and handling of biological material as well as recently developed data storage techniques require methods that provide a spatial resolution beyond the diffraction limit of light microscopy. The atomic force microscope (AFM) [2] has become one of the most important tools to address the nanometer scale and is used for imaging applications [4] as well as for surface characterization [15], lithography [11], data storage [6], and handling of nanometer sized particles [9]. Generally, the advantage of highest-resolution is diminished by the slow imaging speed. Therefore, a crucial issue in AFM development is to increase the speed, which is limited by the dynamic behavior of the moving parts, i.e. the cantilever in tapping-mode [23], the scanning unit [3,19], and the actuator for topographical feedback [18]. Recent developments were done to speed up the AFM by focussing on the mechanical design [12], implementing multiple actuator systems [13], and by applying modern control methods [3,17,5,20]. However, one restriction that is common to all scanning probe microscopes (SPM) is the limited imaging speed due to the sequential raster scanning of the tip or sample in order to acquire one image. This scanning motion is limited in speed due to the mechanical behavior of the scanning unit (cf. [19]). Some effort has been done to speed up these systems by building fast scanners for scanning tunnelling microscopes (STM) and AFMs, where the approach to scale the system down [14] is very common. A recent paper [16] shows a design that is based on shear piezos to perform the scanning motion, which is a very elegant solution for high-speed STM but limits applications for AFM imaging due to its small scan range. Ando et al. [1] presented a high-speed AFM design, where the different positioning axes are stacked on top of each other. Although, imaging at speeds of up to 1200 lines per second has been achieved, this AFM is limited in its usability by a small scan range and due to the fact that the fast scanning direction is predefined by the mechanical design. Another approach for high-speed imaging has been demonstrated by scanning at the

* Corresponding author. Address: Delft University of Technology, Delft Center for Systems and Control, Mekelweg 2, 2628 CD, Delft, The Netherlands. Tel.: +31 15 27 86152; fax: +31 15 27 86679.
E-mail address: g.schitter@tudelft.nl (G. Schitter).

0957-4158/$ - see front matter © 2008 Elsevier Ltd. All rights reserved.
doi:10.1016/j.mechatronics.2008.02.007

resonance of the scanner [10]. This solution also is limited to a predefined fast scanning direction and the fact that the scanning motion is sinusoidal rather than the preferred triangular scanning motion. This results in a varying tip-speed and tip–sample interaction, and in the requirement to de-convolute the images due to the varying pixel distances when acquiring the image.

In this paper we present a novel mechanical design of an AFM scanner that is based on piezoelectric stack actuators and a flexure mechanism that decouples the axes of motion and clamps the actuators on both sides in order to shorten the mechanical paths to a functional minimum. In Section 2 we present the mechanical design of this mechatronic system. Section 3 discusses the system dynamics and limitations in the scanning direction. In Section 4 a new method based on input-shaping techniques to compensate the system dynamics is presented and proven experimentally. Imaging results are presented demonstrating the high-speed imaging capability of the new AFM.

2. Scanner design

2.1. Basic mechanical design

The core piece of the new design of the high-speed AFM is the scanning unit, which consists of piezoelectric stack actuators and a flexure mechanism that enables decoupling of the different axes of motion while keeping the mechanical structure stiff. Stiffness is important in order to achieve high fundamental resonance frequencies in the respective positioning direction for highest performance of the new scanning device. Fig. 1 shows a scheme of the scanner design. The Z-actuator (for vertical positioning) is mounted on a center piece that is moved by the X and Y piezos (for lateral positioning). The small parallel flexures (comb-flexures) that connect the center piece with the inner frame (deformed black square connected to the support material) decouple the X and Y motion. The inner frame is flexible in the actuation direction of the respective piezo and is stiff in the two perpendicular directions. This confines the possible movement of the piezo to its actuation direction [8] and suppresses out of plane and torsional motion of the respective actuator. Simultaneously this inner frame serves as rigid support of the Z-actuator by reducing the mechanical path length of the Z-actuator's support. This shifts the fundamental resonance frequency in the Z-direction towards much higher frequencies and suppresses trampoline motion of the scanning system in the Z-direction. The scanning actuators in the X- and Y-directions are arranged in the so called "push–pull principle" (see Fig. 1); for each scanning direction pairs of piezos are arranged to opposite in phase with each other in order to form a balanced structure. Besides the fact that two piezos provide more force than one, this has the advantage that the scanning actuation is mechanically balanced and the recoil in the supporting structure gets minimized. Furthermore, this arrangement of the actuators is thermally balanced, which reduces the thermal drift for stable imaging at highest-resolution, and allows the implementation of a strain gage full-bridge circuit that is also thermally balanced.

2.2. Finite element analysis and implementation

In order to achieve an increased scan-range in the X- and Y-directions with maximum stiffness in the Z-direction, we chose to implement two pairs of piezos for each scanning direction. The push–pull structure in the X-direction is comprised of four piezos with dimensions of $5 \times 5 \times 10$ mm. The same assembly is used for the Y-direction. These eight piezos are integrated into the supporting structure and center piece (cf. Figs. 2 and 3) to form the scanner assembly. The center piece, which includes all flexures and the two frames that stiffen the system in the Z-direction (see Fig. 3), consists of aluminium to reduce the moved mass and increase flexibility while providing sufficient stiffness. The Z-actuator is mounted on top of the center piece.

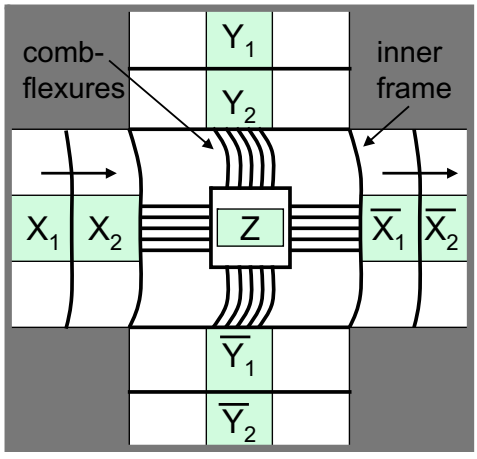

Fig. 1. Flexure based high-speed scanner. Piezoelectric stack actuators provide the movement in the individual directions.

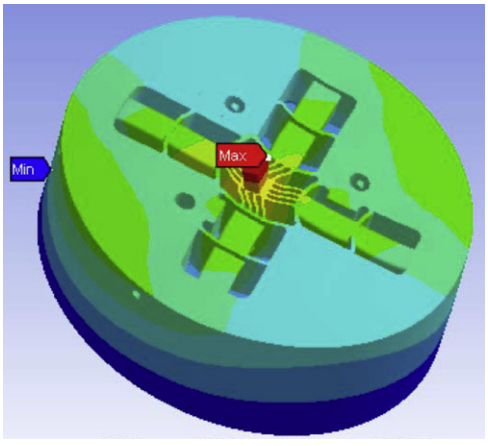

Fig. 2. FEA simulation showing the first mode of the scanner in the X- and Y-directions at 26.7 kHz.

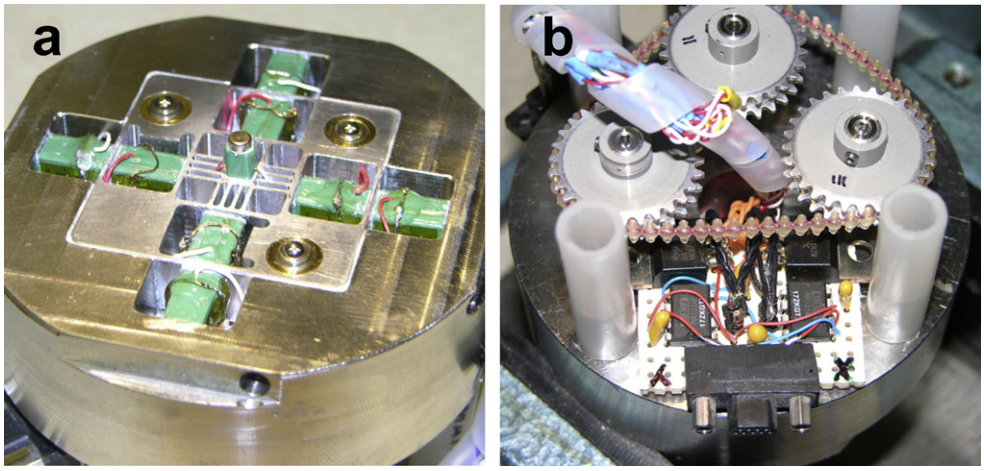

Fig. 3. Implementation of the high-speed scanner. In the top-view (a) the flexures and the scanning piezos are clearly visible. The bottom view (b) shows the belt driven screws for the parallel approach and the electronic circuit for the read-out of the strain gage signal.

In order to achieve maximum stiffness for the outer support of the scanning piezos and to hold the aluminium center piece, the outer housing is made of stainless steel. Three 200 tpi screws (Azeer Enterprises, Landing, NJ) are integrated into the scanner to hold the AFM head (including the AFM cantilever) by a kinematic mount. Coupling all three screws with a belt drive allows a parallel approach of the cantilever onto the sample surface. The actual design of the scanner has been done in several iterations using modern design software (Solid Edge, UGS, Plano, TX) and evaluating it with finite element analysis (FEA) tools (Ansys, Canonsburg, PA). Fig. 2 shows the FEA predicted first resonance frequency of the new scanner in the scanning direction, which is predicted to occur at 26.7 kHz. This mode is a coupled oscillation between the X- and the Y-directions. If uncompensated this coupled mode may not only impair the tracking accuracy in the respective scanning direction, but may also increase the cross-coupling into the other scanning direction at this frequency, therefore causing increased imaging artifacts (cf. Section 4). The first resonance that occurs in only one scanning direction (not shown) is at 34 kHz. The first resonant mode in the Z-direction is predicted to occur at 33 kHz [21].

The resulting design eventually has been built as shown in Fig. 3. The top-view (Fig. 3a) shows the Z-piezo (AE0203D04, Tokin-NEC, Sendai City, Japan) glued onto the center piece and the eight scanning piezos (AE0505D08, Tokin-NEC) integrated in the aluminum center piece and steel housing. Strain gages are glued on each scanning piezo, which are combined to form a full-bridge circuit for read-out of the X- and Y-position, respectively. Since the signal of the strain gage bridge is in the mV-range an instrumentation amplifier is attached as closely as possible to the strain gages (Fig. 3b), in order to enhance the measured signal and minimize the accumulated noise. Fig. 3b also shows the belt drive of the 200 dpi screws for the parallel approach.

The piezos are driven by a custom-made power amplifier (TechProject, Vienna, Austria) that is specially designed for the specific capacitive load of the piezos. The requirements to this amplifier are high currents (a few Ampere) and high-bandwidth (>10 kHz) for maximum system performance, while keeping a flat frequency response and a low noise level (<10 mV_{pp}) for highest imaging resolution of the AFM. The symmetric design of the scanner allows full image rotation, i.e. the fast scanning direction can be chosen in any arbitrary direction in the X–Y-plane. The strain gage bridge circuits can be used for closed-loop control of the scanner, e.g. for point and shoot manipulation or single molecule pulling at a user-defined location on the sample surface.

3. System dynamics

The scanner is characterized in the X- and Y-direction for assessment of the achieved system performance. The frequency response is measured with a network analyzer (4395A, Agilent, Palo Alto, CA). The input to the system is the channel of the power amplifier in the respective positioning axis, the system output is the strain gage signal of the corresponding positioning axis. The measurement circuit is sketched in Fig. 4. If switch S_1 is closed, the system is operated at maximum bandwidth for highest performance of the scanning unit. If S_1 is open a 50 Ω resistor is switched in series to each of the piezos in the respective scanning direction. These resistors are for protection of the individual channels of the power amplifier by limiting its output currents. Fig. 5 shows the bode plot of the scanning system in X-direction with switch S_1 closed (solid black line) and open (dashed red line), respectively. If S_1 is closed the system is operated at the full bandwidth. The amplitude spectrum clearly shows the system's first resonance at 22 kHz. Below this frequency the bode plot shows no dynamics of the scanner system. The difference between the FEA predicted resonance at 26.7 kHz and

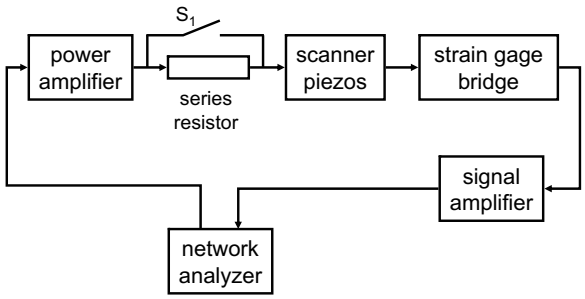

Fig. 4. Measurement circuit for characterization of the scanner in the X- and Y-direction. Switch S_1 is to operate the system with and without the series resistor.

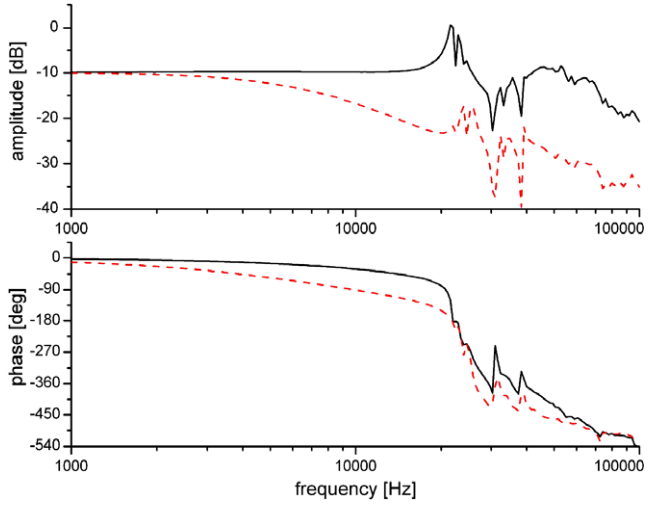

Fig. 5. Bode plot of the scanner in X-direction without series resistor (solid black line) and with a 50 Ω series resistor (dashed red line). The AFM power amplifier electronics is the system input, the signal of the strain gage bridge circuit is regarded as the system output. (For interpretation of the references in colour in this figure legend, the reader is referred to the web version of this article.)

the actual resonance at 22 kHz is due to tolerances when manufacturing the scanner parts and due to uncertainties in some material parameters that had to be estimated for the FEA simulation. At this frequency range two neighbouring peaks can be observed in the amplitude spectrum and the phase lag drops by 360°, which denotes that closed-loop operation of the scanner is limited to below this bandwidth. At 30 kHz the amplitude spectrum clearly shows a sharp anti-resonance, and at about 34 kHz the next resonant behaviour can be observed. With a 50 Ω resistor in series with each scanning piezo, i.e. S_1 is open, the bode plot of the scanner system changes (dashed red line). These resistors not only limit the output current of the power amplifier but simultaneously serve, in combination with the capacitance of the respective piezo, as a low-pass filter, thus limiting the bandwidth of the scanning system. The cut-off frequency of this low-pass filter is at about 8 kHz. At the first resonance frequency of about 22 kHz the system response is already in the low-pass regime, enabling imaging with reduced artifacts stemming from the scanner dynamics (cf. [19]). The low-pass introduced by the series resistor causes an additional phase lag of 90°, further reducing the maximum bandwidth for feedback operation.

4. Scanning signals and control

For imaging at high-speed typically an open-loop operation of the scanning motion is applied. Due to the higher harmonic components of the triangular scanning signal the scanner's resonance is excited when scanning at these high line-scan rates. To avoid turn-around ripples due to the scanner's resonance frequency a new and simple compensation method can be used (Fig. 6). The feasibility of this compensation method is demonstrated by a Matlab/Simulink (The MathWorks Inc., Natick, MA) simulation shown in Fig. 6a, b, d, and e and proven experimentally in Fig. 6c and f. The simulation is based on the measured dynamics of the scanning unit shown in Fig. 5. When the scanning motion is reversed the higher frequency components of the triangular guidance signal (Fig. 6a) excite the lateral dynamics of the scanner, which, in a first approximation, can be regarded as a spring-mass oscillator defined by its resonance frequency $f_0 = 22$ kHz and damping coefficient $\zeta = 0.1$. These oscillations are superimposed on the triangular scan (Fig. 6b) and distort the image (Fig. 6c). By cutting the sharp top of the triangular guidance signal (Fig. 6d) such that the plateau has a length equal to half the period ($T/2$) of the scanner's resonance, one can significantly reduce excitation of these dynamics. Due to its inertia, the scanner cannot follow the abrupt stop of the guidance signal, and starts to oscillate at its resonance frequency. After $T/2$ the scanner returns to the same position and has about the same speed, but is traveling in the opposite direction, as it was when the guidance signal stopped rising. At this point the guidance signal starts falling with the same speed, enabling a smooth transition without exciting the scanner dynamics. In this case the actual scanning motion has a constant speed over the most part of the scanned area and differs from the desired imaging speed only at the fringes of the image (Fig. 6f), where the scanning motion describes a sinusoidal half wave of the scanner's natural oscillation. To avoid excitation of the higher frequency dynamics of the scanner (destabilization of a higher mode), and to smooth the D/A converted scanning signals, these signals are low-pass filtered with a cut-off frequency of 40 kHz.

This approach is related to input-shaping techniques (see e.g. [22] and references therein), and the required guidance signal can be generated without the need to implement an explicit controller, simply by cutting the top of the triangular scanning signal. The scanning signals are generated by the data acquisition (DAQ) system [7] of our prototype AFM. The modification to shape the input of the scanning signal is added onto an advanced version of this DAQ system. Alternatively to the input-shaping one could also

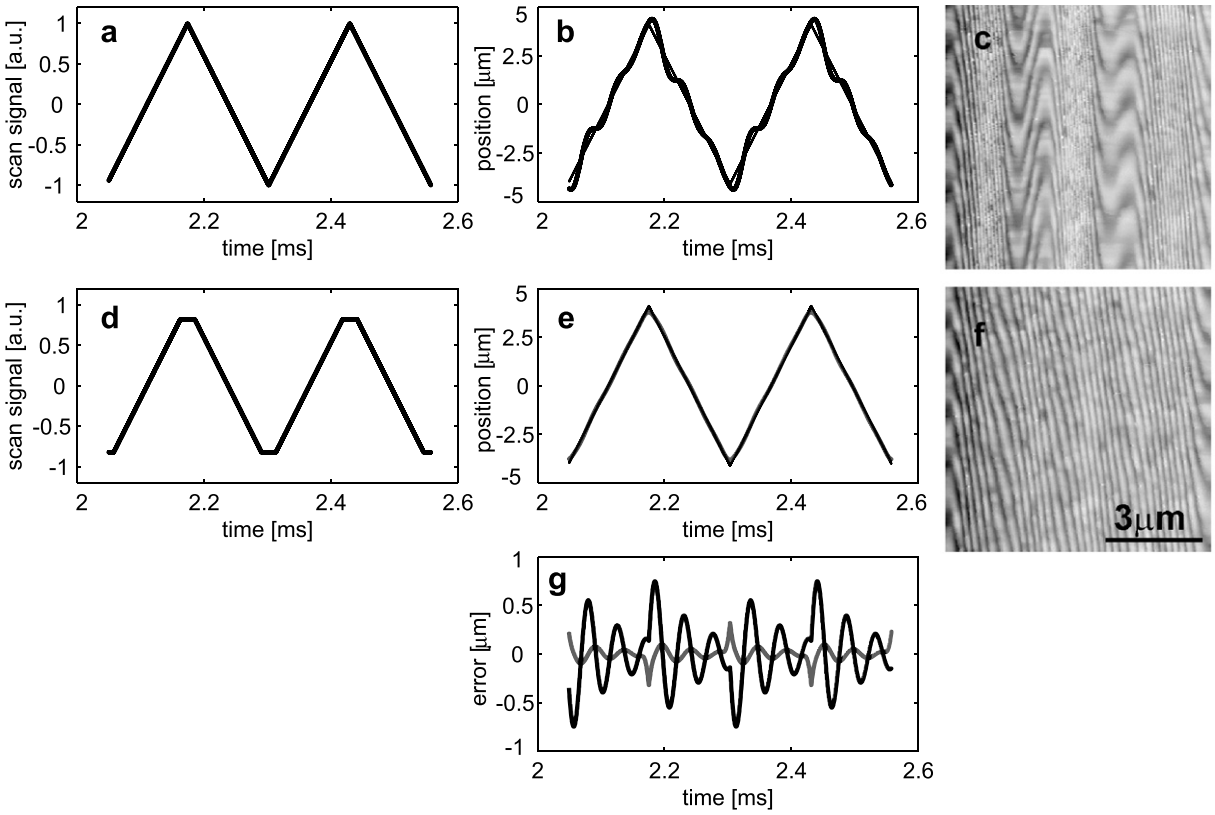

Fig. 6. Triangular scanning signal (a) at a line-scan rate of 3910 Hz. The scanner is excited at its resonance frequency, simulated in (b), resulting in distortion of the AFM images (c). Modified scan signal to compensate the resonant behavior of the scanner (d), and resulting scanning motion due to the inertia of the scanner, simulated (e). The image distortion is reduced (f) and the center of the scanned area appears linear. A comparison of the tracking error of the triangular scan (black) and the modified scan (gray) is shown in (g). AFM images (c) and (f) show an InP calibration grating (233 nm equally spaced lines) imaged at a line-scan rate of 3910 Hz.

compensate for the scanner dynamics with inversion based methods (e.g. [3,19]). However, the additional advantages of the input-shaping approach are that the simple knowledge of the scanner's resonance frequency is sufficient to compensate for most of the scanner dynamics, without the need to model the full system dynamics, and that one can use this method also at line-scan rates exceeding 20% of the scanner's resonance.

Fig. 6g shows a comparison of the positioning error of the scanning motions shown in Fig. 6b (black line) and Fig. 6e (gray line), respectively. The residual positioning error is significantly reduced by the modified scanning signal, where the highest error-peak occurs at the not trackable sharp tip of the desired triangular trajectory. An even stronger reduction in these errors can be seen from the AFM images (cf. Fig. 6c and f), where the errors causing imaging artifacts are comprised of tracking errors in the respective scanning direction as well as a potential increased cross-talk to the other scanning direction at the first resonance frequency of the scanner (cf. Fig. 2). Although the lateral oscillations of the scanner, due to the mechanical structure, may be stronger at the location of the sample than at the signals of the strain gauge sensor, the sensor signal is in good agreement with the improvement of the imaging performance. Fig. 7 shows an oscilloscope-trace of the scanning signal (dashed blue lines) and the strain gage signal (solid red lines) when scanning at 3910 lines per second. Hysteresis of the piezoelectric actuators has been pre-compensated by adding a weighted (about 7%) sinusoidal signal to the triangular scanning signal (see dashed blue lines in

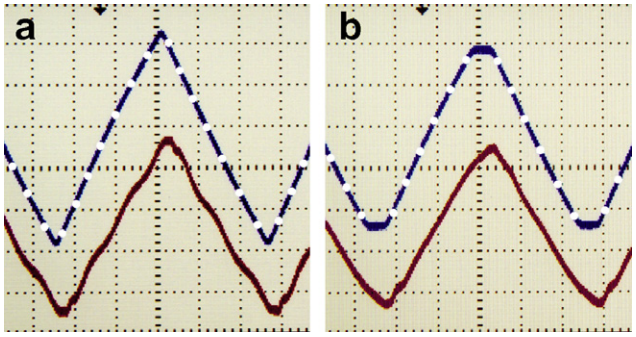

Fig. 7. Scanning motion of the high-speed scanner at a line-scan rate of 3910 Hz (time scale: 50 µs/div). Scanning signal (dashed blue, 500 mV/div.), scanner position (solid red, 200 mV/div.). (a) At a triangular scanning signal oscillations due to the scanner dynamics can be observed. (b) The input-shaped scanning signal reduces scanner oscillations considerably. (For interpretation of the references in colour in this figure legend, the reader is referred to the web version of this article.)

Fig. 7). The line-scan rate is determined by the software of the DAQ system, which allows only certain choices for imaging at high-speed [8]. At more natural line-scan rates, e.g. 4000 lines per second, the error would not be substantial different, since the input-shaping of the scanning motion is adjusted accordingly to always match half a cycle of the scanner's resonance frequency. In Fig. 7a the oscillations due to the scanner's dynamics are superimposed on the desired triangular scanning motion and can clearly be seen in the signal of the strain gage bridge circuit (solid red line). Fig. 7b shows the modified scanning signal (dashed blue line) at a line-scan rate of 3910 Hz and the system response, given by the output of the strain gage bridge circuit (solid red line). The oscillations due to the scanner's dynamics (cf. Fig. 7a) are clearly reduced and can hardly be seen in the signal of the strain gage bridge circuit in Fig. 7b. This compensation mechanism enables high-speed imaging with an improved image quality. Fig. 8 shows images of an InP-grating showing parallel lines at a pitch of 233 nm. These images have been recorded at a speed of 7810 lines per second and a resolution of 128 by 128 pixels per image, corresponding to a frame rate of 61 images per second. In case of the sharp triangular scanning signal (images (a) and (b)) the parallel lines are distorted due to the scanner oscillations, resulting in sinusoidal Moiré-patterns visible in the image. I case of the input-shaped scanning signal (images (c) and (d)) dynamics induced imaging artifacts are minimized and the lines of the grating appear parallel in the center of the image. Distortions of the image only can be observed at the fringes of the image, where the scanning motion is rather sinusoidal than triangular. The residual artifacts, however, can easily be avoided by scanning a larger area and cropping of the non-linear fringes of the image, or by compression of the image at its fringes for deconvolution of this area.

Images were recorded in contact mode using small cantilevers (SCL-Sensor. Tech., Deutsch-Wagram, Austria) with a nominal spring constant of $k < 0.1$ N/m and a free resonance frequency of $f_0 > 200$ kHz. Feedback operation of the tip–sample interaction has been done with an analogue proportional integral (PI) feedback controller in order to keep the cantilever deflection, and thus the imaging force, constant.

Fig. 9 shows AFM images of a bovine bone specimen (images a–c) and a calibration grating (image d) recorded at different line-scan rates. The low-pass characteristics when operating the scanner with the series resistors can be observed by the non-square appearance of the etched structure in the calibration grating. This can be compensated by adjusting the ratio of the scanning signals applied in the X- and Y-directions, respectively.

In summary the images acquired with the new scanner and improved scanning signal demonstrates feasibility of AFM imaging at video-rates.

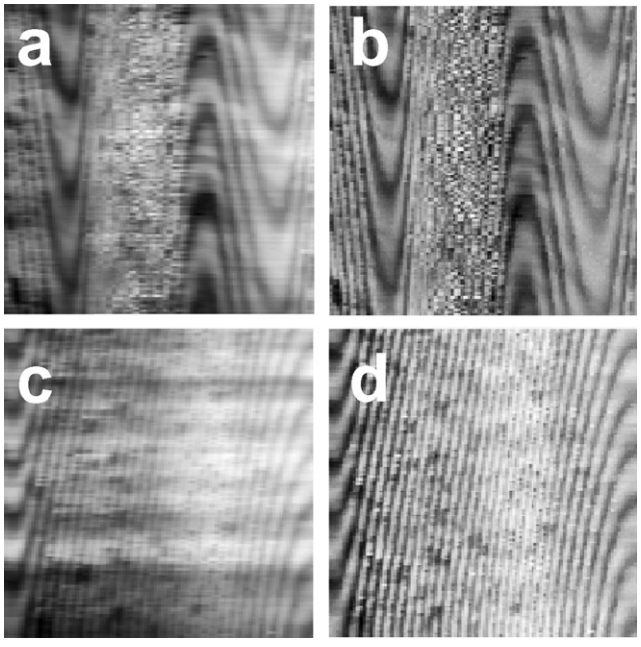

Fig. 8. Topography images (a and c) and deflection images (b and d) of an InP-grating showing parallel lines at a pitch of 233 nm, imaged at 7810 lines per second. Images (a) and (b) were recorded while scanning with a sharp triangular scanning signal, whereas images (c) and (d) are recorded during imaging with the input-shaped scanning signal.

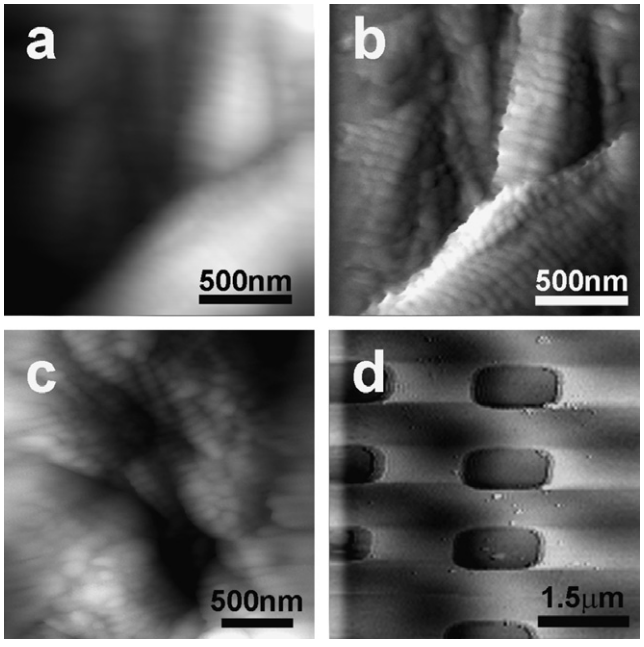

Fig. 9. (a) Topography and (b) deflection image of a native surface of a single trabecula from a bovine bone femur, imaged at a line-scan rate of 1030 Hz and a resolution of 256 by 256 pixels. The image shows collagen fibrils with their characteristic 67 nm banding pattern. (c) Deflection image of the same specimen, recorded at 3910 Hz line-scan rate and a resolution of 256 by 256 pixels. (d) Deflection image of a silicon calibration grating with 44 nm deep etched squared holes at a pitch of 3 μm, imaged at a line-scan rate of 7810 Hz and a resolution of 128 by 128 pixels, corresponding to 61 images per second.

5. Conclusions

This paper presents a new scanner design for high-speed atomic force microscopy. The advanced mechanical design is optimized utilizing FEA tools. The dynamic behaviour of the actual built scanning unit is characterized and agrees well with the FEA predicted dynamics. An input-shaping based control method is presented that compensates the main dynamics of the high-speed scanner. The performance of this new AFM system is demonstrated by imaging test samples at speeds of up to 61 frames per second. Future work will be focussed on the implementation of model-based controllers [20] to improve the control bandwidth in the vertical direction, and implementation of iterative learning controllers [24] for an improved shaping of the scanning motion based on information gathered from the lateral position sensors.

In summary, this new AFM system enables imaging speeds that are three orders of magnitude faster than conventional AFM systems. This is an important step towards real-time observation of dynamic chemical and biological processes on the molecular level with the AFM.

Acknowledgements

This work has been supported by SNF-fellowships PA002-108933 and PA002-111445, by faculty 3mE Grant PAL614, by a research agreement with Veeco #SB030071, and by the National Institutes of Health under Award RO1 GM 065354.

References

[1] Ando T, Kodera N, Takai E, Maruyama D, Saito K, Toda A. A high-speed atomic force microscope for studying biological macromolecules. Proc Nat Acad Sci USA 2001;98(22):12468–72.
[2] Binnig G, Quate CF, Gerber Ch. Atomic force microscope. Phys Rev Lett 1986;56(9):930–3.
[3] Croft D, Shed G, Devasia S. Creep, hysteresis, and vibration compensation for piezoactuators: atomic force microscopy application. ASME J Dyn Syst, Meas, Control 2001;123:35–43.
[4] Drake B, Prater CB, Weisenhorn AL, Gould SAC, Albrecht TR, Quate CF, et al. Imaging crystals, polymers, and processes in water with the atomic force microscope. Science 1989;243(4898):1586–9.
[5] El Rifai OM, Youcef-Toumi K. Trade-offs and performance limitations in mechatronic systems: a case study. Ann Rev Contr 2004;28(2):181–92.
[6] Eleftheriou E, Antonakopoulos T, Binnig GK, Cherubini G, Despont M, Dholakia A, et al. Millipede – a mems-based scanning-probe data-storage system. IEEE Trans Magn 2003;39(2):938–45.
[7] Fantner GE, Hegarty P, Kindt JH, Schitter G, Cidade GAG, Hansma PK. Data acquisition system for high speed atomic force microscopy. Rev Sci Instrum 2005;76(2):026118.
[8] Fantner GE, Schitter G, Kindt JH, Ivanovb T, Ivanova K, Patel R, et al. Components for high speed atomic force microscopy. Ultramicroscopy 2006;106:881–7.
[9] Guthold M, Matthews G, Negishi A, Taylor RM, Erie D, Brooks FP, et al. Quantitative manipulation of dna and viruses with the nanomanipulator scanning force microscope. Surf Interf Anal 1999;27(5–6):437–43.
[10] Humphris ADL, Miles MJ, Hobbs JK. A mechanical microscope: high-speed atomic force microscopy. Appl Phys Lett 2005;86(3):034106.
[11] Kim Y, Lieber CM. Machining oxide thin-films with an atomic force microscope – pattern and object formation on the nanometer scale. Science 1992;257(5068):375–7.
[12] Kindt JH, Fantner GE, Cutroni JA, Hansma PK. Rigid design of fast scanning probe microscopes using finite element analysis. Ultramicroscopy 2004;100(3–4):259–65.
[13] Manalis SR, Minne SC, Quate CF. Atomic force microscopy for high speed imaging using cantilevers with an integrated actuator and sensor. Appl Phys Lett 1996;68(6):871–3.
[14] Pohl DW. Some design criteria in scanning tunneling microscopy. IBM J Res Develop 1986;30(4):417–27.
[15] RosaZeiser A, Weilandt E, Hild S, Marti O. The simultaneous measurement of elastic, electrostatic and adhesive properties by scanning force microscopy: pulsed-force mode operation. Meas Sci Technol 1997;8(11):1333–8.
[16] Rost MJ, Crama L, Schakel P, Van Toll E, Van Velzen-Williams GBEM, Overgauw CF, et al. Scanning probe microscopes go video rate and beyond. Rev Sci Instrum 2005;76:053710.
[17] Salapaka S, Sebastian A, Cleveland JP, Salapaka MV. High bandwidth nano-positioner: a robust control approach. Rev Sci Instrum 2002;73(9):3232–41.
[18] Schitter G, Menold P, Knapp HF, Allgöwer F, Stemmer A. High performance feedback for fast scanning atomic force microscopes. Rev Sci Instrum 2001;72(8):3320–7.
[19] Schitter G, Stemmer A. Identification and open-loop tracking control of a piezoelectric tube scanner for high-speed scanning probe microscopy. IEEE Trans Contr Syst Technol 2004;12(3):449–54.
[20] Schitter G, Stemmer A, Allgöwer F. Robust two-degree-of-freedom control of an atomic force microscope. Asian J Contr 2004;6(2):156–63.
[21] Schitter G, Åström K, DeMartini BE, Thurner PJ, Turner KL, Hansma PK. Design and modeling of a high-speed AFM-scanner. IEEE Trans Contr Syst Technol 2007;15(5):906–15.
[22] Singhose WE, Seering WP, Singer NC. Improving repeatability of coordinate measuring machines with shaped command signals. Precis Eng – J Am Soc Precis Eng 1996;18(2–3):138–46.
[23] Sulchek T, Yaralioglu GG, Quate CF, Minne SC. Characterization and optimization of scan speed for tapping-mode atomic force microscopy. Rev Sci Instrum 2002;73(8):2928–36.
[24] Wu Ying, Zou Qingze. Iterative control approach to compensate for the hysteresis and the vibrational dynamics effects of piezo actuators. In: Proc IEEE 2006 American Control Conference, Minneapolis, MN, USA, June 2006. p. 424–9.